Case Studies in Thermal Engineering 26 (2021) 100975

Contents lists available at ScienceDirect

Case Studies in Thermal Engineering

journal homepage: http://www.elsevier.com/locate/csite

Heat and mass transfer in MHD Williamson nanofluid flow over an exponentially porous stretching surface

Yi-Xia Li [a], Mohammed Hamed Alshbool [b], Yu-Pei Lv [c,*], Ilyas Khan [d,**], M. Riaz Khan [e,***], Alibek Issakhov [f,g]

[a] College of Mathematics and Finance, Xiangnan University, Chenzhou 423000, PR China
[b] Department of Applied Mathematics, Abu Dhabi University, Abu Dhabi 59911, United Arab Emirates
[c] Department of Mathematics, Huzhou University, Huzhou 313000, PR China
[d] Department of Mathematics, College of Science Al-Zulfi, Majmaah University, Al-Majmaah, P.O. Box 66, Majmaah 11952, Saudi Arabia
[e] LSEC and ICMSEC, Academy of Mathematics and Systems Science, Chinese Academy of Sciences; School of Mathematical Science, University of Chinese Academy of Sciences, Beijing 100190, PR China
[f] Department of Mathematical and Computer Modeling, Al-Farabi Kazakh National University, Almaty, Kazakhstan
[g] Department of Mathematical and Computer Modeling, Kazakh British-Technical University, Almaty, Kazakhstan

A R T I C L E I N F O

Keywords:
Williamson nanofluid
Exponential stretching
Porous medium
Suction
Aligned magnetic field
Heat generation/absorption

A B S T R A C T

The present study investigates the rate of heat and mass transfer in MHD Williamson nanofluid flow over an exponentially porous stretching surface subject to the heat generation/absorption and mass suction. The analysis has been carried out for the two different conditions of heat transfer stated as prescribed exponential order surface temperature (PEST) and prescribed exponential order heat flux (PEHF). Moreover, an exterior magnetic field is applied with an inclined angle along the stretched surface. Mathematically, the existing flow problem has been configured in accordance with the fundamental laws of motion and heat transfer. The similarity transformations have been used to transform the governing equations into the nonlinear ordinary differential equations (ODEs). The numerical solution to the resulting nonlinear ODEs with the associated boundary conditions have been obtained with the utilization of bvp4c package in MATLAB. The behavior of the resulting equations of the problem is checked graphically under the influence of various flow parameters which ensures that the rate of heat transfer decreases with the increase of Brownian motion parameter as well as it increases with the increase of thermophoresis parameter. Moreover, the Sherwood number increases with the rising values of the Prandtl number and Lewis number.

1. Introduction

In several realistic conditions, it is not essential that the surface must be linear, such as in the stretching of plastic sheet. The evaluation of heat transfer across a boundary layer flow through a continuous stretched surface subject to the prescribed heat flux and

Abbreviations: 74Axx, 76Bxx; 76Nxx, 65Nxx.

* Corresponding author.
** Corresponding author.
*** Corresponding author.
E-mail addresses: peipei@zjhu.edu.cn (Y.-P. Lv), i.said@mu.edu.sa (I. Khan), mrkhan.math@hotmail.com (M. Riaz Khan).

https://doi.org/10.1016/j.csite.2021.100975
Received 13 March 2021; Received in revised form 28 March 2021; Accepted 29 March 2021
Available online 1 April 2021

surface temperature has been reached to a significant interest in view of its importance in industrial processing of glass fiber, metal wires, polymer sheets, paper production and plastic films. In polymer, the rate of cooling is highly dependent on the feature of the resulting product in manufacturing of plastic and glass. The flow of the boundary layer across a continuous stretched surface was initially studied by Sakiadis [1] by providing the boundary layer equations in two dimensions. The assessment of heat transfer across a boundary layer flow subject to the stretched surface was explored by Tsou et al. [2]. The same work was extended by Erickson et al. [3] to check the mass transfer with the consideration of suction and injection. In this way, multiple scholars have shown their interest in the flow of boundary layer across a linear stretched surface [4–6]. Khan M. R. et al. [7] planned the flow of CNTs water nanofluid for the comparative study of heat transfer across a curved stretching surface. Nadeem et al. [8] investigated the features of heat transfer in the flow of nanofluid including an oblique stagnation point with oscillatory stretching/shrinking surface. The study of mass transfer and Newtonian heating for the flow of mixed convection Walters-B nanofluid subject to the stretched surface was projected by Qaiser D. et al. [9]. Khan M. R. et al. [10] determine the dual solution for the flow of hybrid nanofluid assuming the existence of mixed convection along a curved stretching/shrinking surface.

Initially, the study of magneto-hydrodynamics (MHD) was reported in geophysical and astrophysical problems. During the last several years, this topic has come to the special focus based on their variety of applications in the medical, engineering, and petroleum-refining sectors. The existence of MHD in the nanofluid flow of three-dimensional coordinate was planned by Sheikholeslami and Ellahi [11]. It was detected that the presence of MHD raises the resistive (drag) force and minimize the convection current. Additionally, the heat transfer rate is visible to be developed. The thermophysical properties of carbon nanotubes in MHD flow across a moving sheet have been addressed by Haq et al. [12]. It seems that the strength of the magnetic field escalates the fluid temperature. The channel flow of the rotating fluid describing the effect of the transversal magnetic field was recently studied by Mehmood et al. [13], which declares that the force of the magnetic field decays the wall flux. The oblique stagnation point flow with steady MHD forces was addressed by Borrelli et al. [14]. It was highlighted that if the strength of the electric field disappears, at that time the magnetic field occupies the plane of the stream rather than in the parallel direction to the flow. Additionally, the flow of the oblique stagnation point occurs solely when the applicable magnetic field is in the direction of dividing streamlines. Nadeem et al. [15] investigated the two-dimensional viscous flow of a nanofluid relating to the effect of magnetic field across a curved surface. The flow investigations of an electrically conductive liquid with the existence of a magnetic field is of great importance in the current metallurgic industrial processes that lying in the refinement of melted metals, nuclear reactors cooling and in several more manufacturing systems. Pal and Mandal [16] investigated an electrically conducting MHD boundary layer flow of a nanofluid across a nonlinear stretching/shrinking surface considering the existance of Ohmic heating, thermal radiation as well as heat generation/absorption. They determined the existence of dual solutions for the greater values of heat generation/absorption parameter. Although they have restricted their studies for the deliberation of combined influence of magnetic field and thermal radiation on the flow of nanofluid across a porous stretched surface. Some other studies regarding MHD flows are [17–22].

Nanofluid is a combination of base fluid like water with the nanometer-sized particles. It is widely acknowledged that the existence of nanoparticles modifies the transport properties as well as refines the performance of heat transfer of nanofluids. The features of heat transfer of a nanofluid is dependent on the volume fraction and the thermophysical properties of a nanoparticles, as well as it depends on the base fluid thermophysical properties. The existence of magnetic field in the boundary layer flow of a nanofluid possess large number of real-world applications in multiple industrial and engineering fields such as in oil survey, metal extrusion, fiber glass, polymer processing, hot rolling, stretching of plastic foil, and geothermic energy extraction. The nanofluid incorporated with a permeable medium yields good potential in boosting thermal capacity. An excellent procedure for the development of heat transfer rate is the utilization of nanoparticles distributed in the base liquids, such as oil, water, and ethylene glycol [23]. This pioneering approach was initially presented by Choi [24] employing the suspension of nanoparticles in the base liquid for the purpose of improving the heat transfer rate in a nanofluids. Subsequently, Boungiorno [25] explained the cause of heat transfer augmentation of a nanofluids and determined that the influence of Brownian diffusion and thermophoresis are especially accountable for the enhancement of heat transfer. As a result of this new concept, Kuznetsove and Nield [26] and Nield and Kuznetsove [27] have established the double diffusive boundary layer flow of a nanofluid with natural convection across a smooth surface. These investigations have produced the efficient thermal features based on the concentration and volume fraction of the nanoparticles. Recently, several researchers have considered the nanofluid boundary layer flow with various geometries mentioned in the [28–32].

The flow over a porous medium is particularly significant in the material processing, fuel cell machineries, drying processes, geothermal energy, dribble bed chromatography, oil recovery as well as in several more. The joint effect of mass and heat transfer associated with the magnetohydrodynamic boundary layer flow of a nanofluid across a porous medium is an active technique to advance the thermal performance. In this regard, Chamkha et al. [33] investigated the influence of porous medium and natural convection on the boundary layer flow across an inclined surface concerning to the thermal radiation as well as the non-uniform porosity. The mass and heat transfer investigation of Hadidi et al. [34] through a porous inclined enclosure designated that the average Nusselt number and the flow structure is greatly affected by the permeability of the porous media. The buoyancy-induced flow containing the features of non-Newtonian nanofluids following the model of a third-grade fluid near a porous vertical stretched surface was considered by Khan et al. [35]. They executed the numerical results for the joint phenomenon of heat and mass transfer depending on the convective boundary conditions and the partial slip velocity condition. Moreover, the study of free convective laminar flow of a magnetohydrodynamics nanofluid across a porous vertical stretched surface excluding the influence of thermal radiation has been provided by Freidoonimehr et al. [36].

On the basis of foregoing indicated studies, it is determined that the rate of heat and mass transfer in Williamson nanofluid flow over an exponentially porous stretching surface subject to the exponential order surface temperature and heat flux is not yet studied under the influence of an exterior aligned magnetic field, mass suction and heat generation/absorption. Therefore, to address this gap, it is our intension to examine the influence of aligned magnetic field, and heat generation/absorption on the Williamson nanofluid flow over an exponentially porous stretching surface subject to the exponential order surface temperature and heat flux. In this regard, the research work of Shazwani Md Razi et al. [37] and Nadeem et al. [38] have been extended by adding the aligned magnetic field and heat generation/absorption along a permeable stretched surface. Mathematically, the existing flow problem has been configured in accordance with the fundamental laws of motion and heat transfer. The similarity transformations have been used to transform the governing equations into the nonlinear ODEs. The numerical solution to the resulting nonlinear ODEs with the connected boundary conditions have been found with the utilization of the bvp4c package in MATLAB. The behavior of the resulting equations of the problem is checked graphically under the influence of various flow parameters. These graphical outcomes have been obtained in terms of velocity, temperature, skin friction coefficient, local Nusselt number and the Sherwood number for various physical flow parameters unless the required accuracy level is achieved. It is anticipated that the outcomes of the existing work will prove advantageous in the forthcoming research to upgrade the development in scientific and engineering fields.

2. Basic equations

Consider the steady two-dimensional Williamson nanofluid flow over a stretched porous exponential surface. It was recognized that the sheet is exponentially stretched with the varying velocity U_w in the x-direction as well as the fluid which is occupied in y-direction is governed by the velocity U_w. Moreover, an exterior aligned magnetic field of intensity B_0 is applied with angle β along the stretched surface as well as the suction v_w phenomenon and the existence of heat generation/absorption is considered. With these preconditions, the main boundary layer MHD equations for the continuity, momentum, energy, as well as concentration are respectively defined as [38,39].

$$\frac{\partial u}{\partial x}+\frac{\partial u}{\partial y}=0, \tag{1}$$

$$u\frac{\partial u}{\partial x}+v\frac{\partial u}{\partial y}=\nu\frac{\partial^2 u}{\partial y^2}+\sqrt{2}\nu\Gamma\frac{\partial u}{\partial y}\frac{\partial^2 u}{\partial y^2}-\nu\frac{u}{k_1}-\frac{\sigma B^2}{\rho}\sin^2\beta u, \tag{2}$$

$$u\frac{\partial T}{\partial x}+v\frac{\partial T}{\partial y}=\alpha\frac{\partial^2 T}{\partial y^2}+\frac{Q_0}{(\rho C_p)_f}(T-T_\infty)+\frac{(\rho C_p)_p}{(\rho C_p)_f}\left[D_B\frac{\partial T}{\partial y}\frac{\partial C}{\partial y}+\frac{D_T}{T_\infty}\left(\frac{\partial T}{\partial y}\right)^2\right]. \tag{3}$$

$$u\frac{\partial C}{\partial x}+v\frac{\partial C}{\partial y}= D_B\left(\frac{\partial^2 C}{\partial y^2}\right)+\frac{D_T}{T_\infty}\left(\frac{\partial^2 u}{\partial y^2}\right). \tag{4}$$

The boundary conditions connected to (1–4) are

$$\left.\begin{array}{l} u=u_w=U_0 e^{\left(\frac{x}{l}\right)},\ v_w=-\gamma(x),\ T=T_w,\ C=C_w\ at\ y=0 \\ u=u_e\to 0,\ T\to T_\infty\ ,\ C\to C_\infty\ as\ y\to\infty \end{array}\right\} \tag{5}$$

Here u and v_w individually mark the two parts of velocity in x and y path. Further $k_1,\ \nu,\rho,\sigma,\ T,T_\infty,\ C,C_\infty,\ Q_0$ separately provides the permeability of the porous medium, kinematic viscosity, density, electrical conductivity, temperature, ambient fluid temperature, concentration, ambient nanoparticles volume fraction and the initial value of heat generation coefficient (heat source). Similarly, Γ,α, $(\rho C_p)_p$, $(\rho C_p)_f$, $D_B$and D_T delivers the shear stress, thermal diffusivity, heat capacity, fluid heat capacity, coefficient of Brownian and thermophoresis diffusion respectively.

2.1. Similarity solution of the governing equations

The governing equations (1)–(4) are non-linear PDE's. We use the similarity transformation given below to convert the non-linear PDE's into a non-linear ODE's

$$\left.\begin{array}{l} u=U_0 e^{\frac{x}{l}} f'(\eta),\ \eta=\sqrt{\dfrac{U_0}{2\nu l}}\,y e^{\frac{x}{2l}}\ , \\ v_w=-\sqrt{\dfrac{\nu U_0}{2l}}\,e^{\frac{x}{2l}}[f(\eta)+\ \eta f'(\eta)] \end{array}\right\}. \tag{6}$$

The boundary conditions for the two cases of PEHF and PEST associated with the above equations (1)–(4) are given as.

2.2. PEST case

$$T=T_\infty+(T_w-T_\infty)e^{\frac{x}{2l}}\theta(\eta),\ h=\frac{C-C_\infty}{C_w-C_\infty}. \tag{7}$$

2.3. PEHF case

$$T = T_\infty + \frac{T_w - T_\infty}{K} e^{\frac{x}{2l}} \sqrt{\frac{2\nu l}{U_0}} \varphi(\eta),\ h = \frac{C - C_\infty}{C_w - C_\infty}. \tag{8}$$

In view of the similarity transformation defined above, equation (1) fulfills in identical manner as well as equations (2)–(4) are reduced to the subsequent set of non-linear ODE's

$$f''' - 2(f')^2 + ff'' + \lambda f''' f'' - \left(K + M \sin^2\beta\right) f' = 0\,, \tag{9}$$

2.4. PEST case

$$\theta'' + Pr\left(f\theta' - f'\theta + N_b g'\theta' + N_t \theta'^2 + Q\theta\right) = 0, \tag{10}$$

$$h'' + L_e Pr(fh') + \frac{N_t}{N_b}\theta'' = 0. \tag{11}$$

2.5. PEHF case

$$\varphi'' + Pr\left(f\varphi' - f'\varphi + N_b g'\varphi' + N_t \varphi'^2 + Q\varphi\right) = 0, \tag{12}$$

$$h'' + LePr(fh') + \frac{N_t}{N_b}\varphi'' = 0. \tag{13}$$

Using the similarity transformation into boundary conditions (5), we obtain

$$\left.\begin{array}{l} f(0) = v_w,\ f'(0) = 1 \\ f'(\eta) \to 0\ as\ \eta \to \infty. \end{array}\right\}. \tag{14}$$

Boundary conditions for PEST case

$$\left.\begin{array}{l} \theta(0) = 1,\ h(0) = 1, \\ \theta(\eta) \to 0,\ h(\eta) = 0\ as\ \eta \to \infty. \end{array}\right\}. \tag{15}$$

Boundary conditions for PEHF

$$\left.\begin{array}{l} \varphi'(0) = -1,\ h(0) = 1, \\ \varphi(\eta) \to 0,\ h(\eta) = 0\ as\ \eta \to \infty. \end{array}\right\}. \tag{16}$$

The similarity parameters appeared in above Eqs. 9–16 are N_t, N_b, L_e, Pr, M, λ, K, Q and R_e which respectively represents the thermophoresis and Brownian motion parameter, Lewis number, Prandtl number, Hartmann number, Williamson parameter, porosity parameter, heat source/sink parameter and the Reynolds number. These parameters are defined as

$$\left.\begin{array}{l} N_t = D_B \dfrac{(\rho c)_p}{(\rho c)_f}(C_w - C_\infty),\ N_b = \dfrac{D_T}{T_\infty}\dfrac{(\rho c)_p}{(\rho c)_f}\dfrac{(T_w - T_\infty)}{\nu},\ L_e = \dfrac{\alpha}{D_B},\ Pr = \dfrac{\nu}{\alpha}, \\ M = \dfrac{\sigma B_0}{\rho U_0 e^{\frac{x}{l}}},\ \lambda = \left(\dfrac{U_0}{2}\right)^{\frac{2}{3}} \dfrac{\Gamma}{\sqrt{l}} e^{\frac{x}{2l}},\ K = \dfrac{\nu L}{k_1 U_0} e^{-\frac{x}{l}},\ Q = \dfrac{L Q_0}{U_0 (\rho c_p)} e^{-\frac{x}{l}}\ R_e = \dfrac{U_w L}{\nu} \end{array}\right\}. \tag{17}$$

The friction drags (skin friction coefficient), the heat transfer rate (local Nusselt number) and the Sherwood number have been defined as [39].

$$C_f = \frac{\tau_w}{\rho U_w^2},\ Nu = \frac{x q_w}{k(T_w - T_\infty)},\ Sh = \frac{x q_m}{D_B(C_w - C_\infty)} \tag{18}$$

where τ_w constitute local wall shear stress, q_w is the local heat flux, and q_m is the mass flux which can be determined as

$$\tau_w = \mu\left(\frac{\partial u}{\partial y} + \frac{\Gamma}{\sqrt{2}}\left(\frac{\partial u}{\partial y}\right)^2\right)\Bigg|_{y=0},\ q_w = -k\frac{\partial T}{\partial y}\bigg|_{y=0},\ q_m = -D_B\frac{\partial C}{\partial y}\bigg|_{y=0}. \tag{19}$$

Taking advantage of the similarity variables, the combination of system (18) and (19) provides system (20) as given below

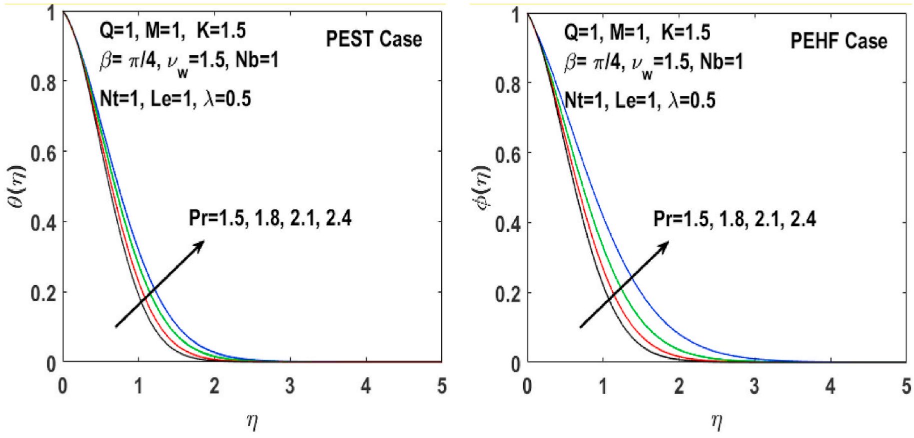

Fig. 1. Temperature $\theta(\eta)$ and $\varphi(\eta)$for different *Pr* values in (a) PEST and (b)PEHF case.

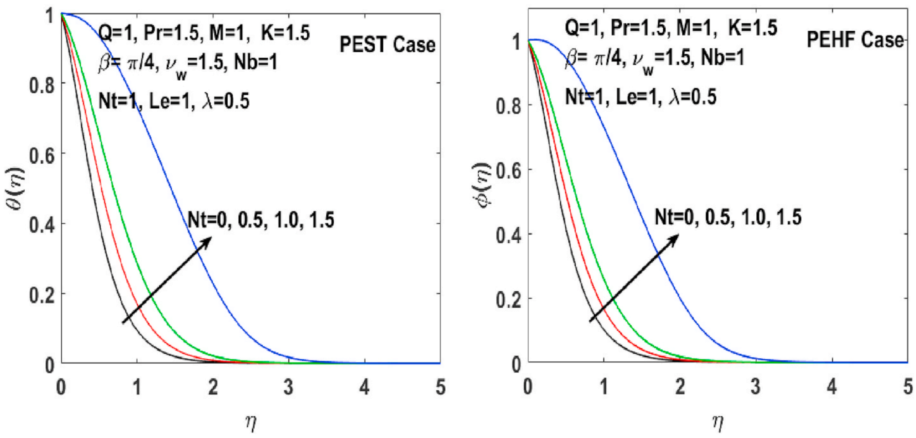

Fig. 2. Temperature $\theta(\eta)$ and $\varphi(\eta)$for different *Nt* values in (a) PEST and (b)PEHF case.

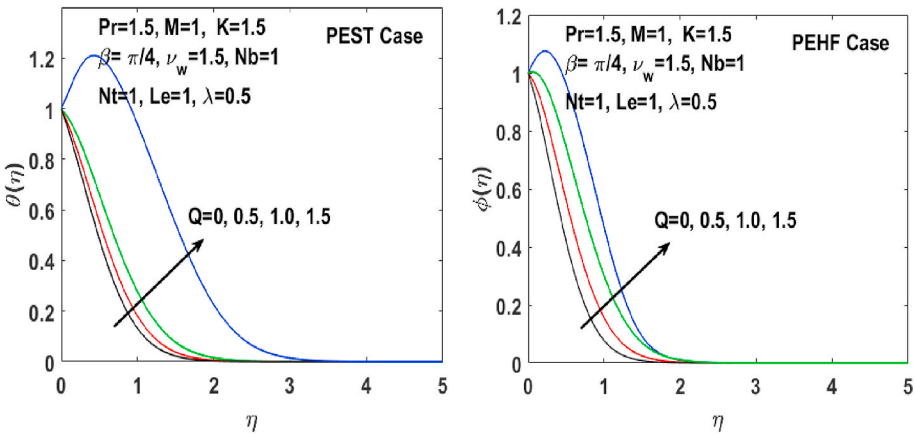

Fig. 3. Temperature $\theta(\eta)$ and $\varphi(\eta)$for different *Q* values in (a) PEST and (b) PEHF case.

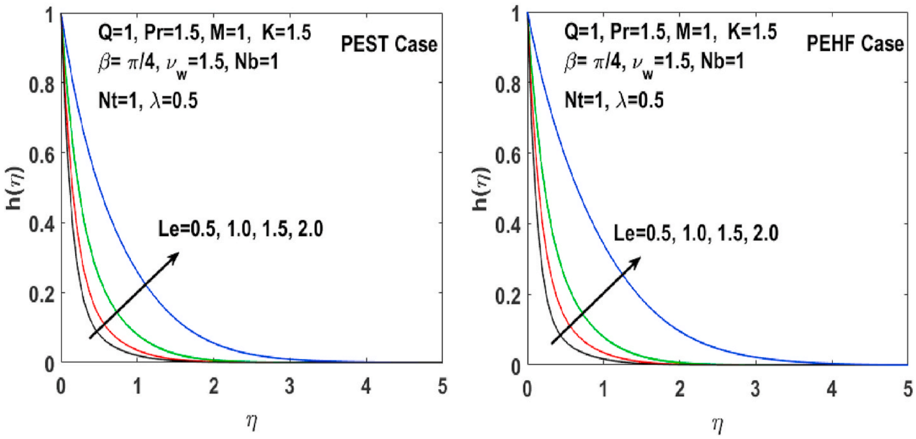

Fig. 4. Concentration h(η) for different *Le* values in (a) PEST case and (b) PEHF case.

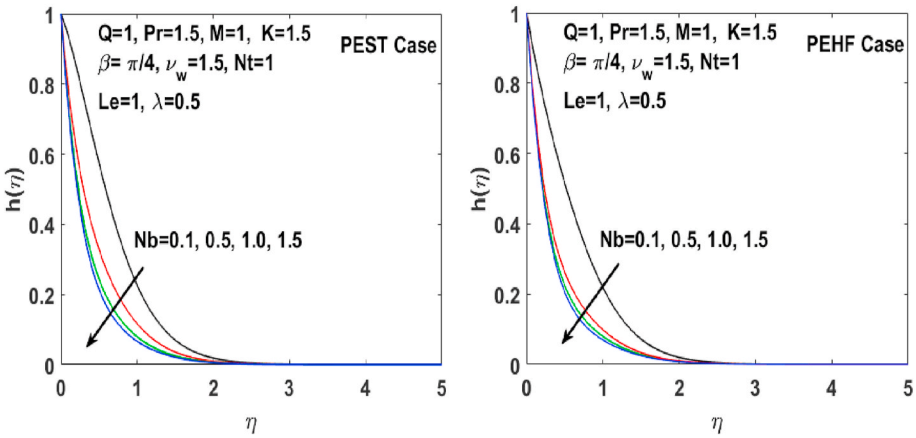

Fig. 5. Concentration h(η) for different *Nb* values in (a) PEST case and (b) PEHF case.

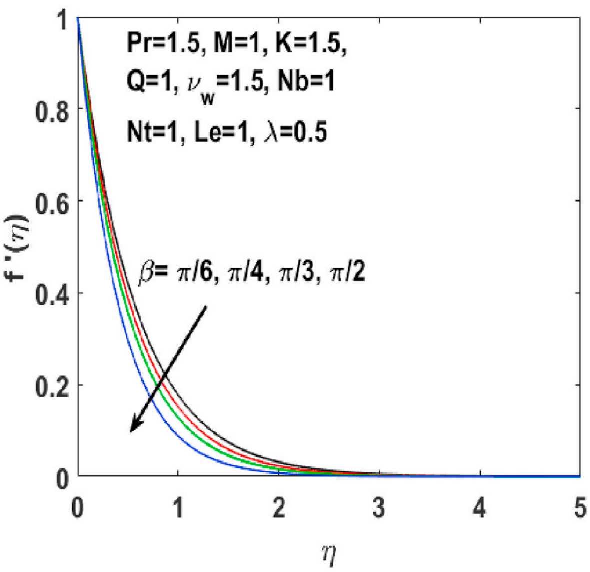

Fig. 6. Velocity $f'(\eta)$ for different β values.

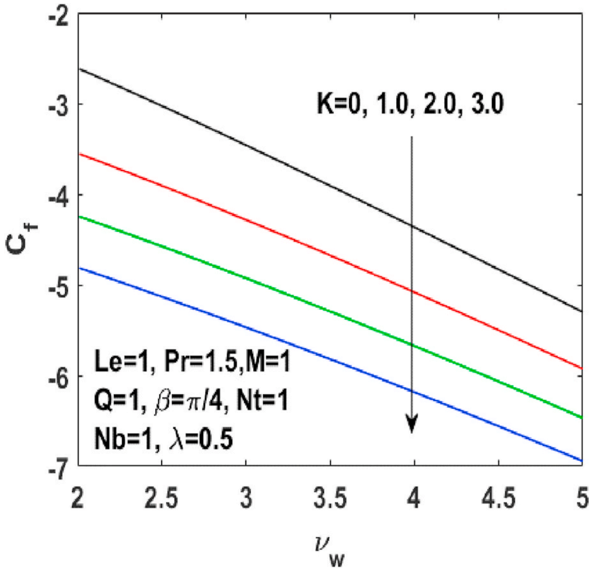

Fig. 7. Friction drag C_f for different K values.

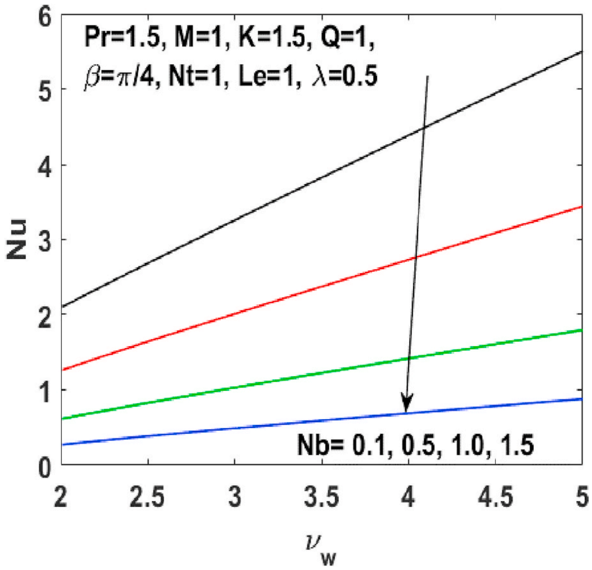

Fig. 8. Nusselt number Nu for different Nb values.

$$\left.\begin{aligned} &(2Re_x)^{1/2}C_f = \left(f'' + \frac{\lambda}{2}f''^2\right)_{\eta=0} \\ &e^{-\frac{x}{2l}}(2Re_x)^{-\frac{1}{2}}Nu = -\theta'(0), \\ &e^{-\frac{x}{2l}}(2Re_x)^{-\frac{1}{2}}Sh = -h'(0), \end{aligned}\right\} \tag{20}$$

3. Results and discussion

This section provides the numerical solution to the resulting nonlinear ODEs (9–13) with the associated boundary conditions (14–16) utilizing the bvp4c package in MATLAB. The behavior of the resulting equations of the problem is checked graphically under the influence of various flow parameters like Pr, N_t, N_b, L_e, β, M, λ, $Q$and K which respectively represents the Prandtl number, thermophoresis and Brownian motion parameter, Lewis number, aligned magnetic field angle, Hartmann number, Williamson parameter,

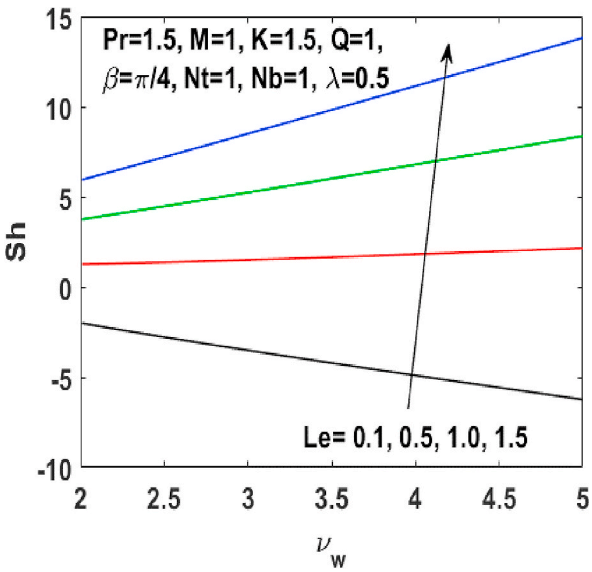

Fig. 9. Sherwood number Sh for different Le values.

Table 1
Comparative values of C_f for different values of λ and v_w.

Present result		Nadeem et al. [39]		
λ	$v_w = 0.1$	$v_w = 0.2$	$v_w = 0.1$	$v_w = 0.2$
0.0	1.23638	1.19298	1.23638	1.19298
0.1	1.20711	1.16468	1.20710	1.16468
0.2	1.17481	1.13364	1.17482	1.13365
0.3	1.13825	1.09880	1.13825	1.09881

heat source/sink parameter and the porosity parameter. The graphical results are obtained in the form of temperature $\theta(\eta)$ and $\varphi(\eta)$, concentration $h(\eta)$, velocity $f'(\eta)$, skin friction coefficient (friction drag), local Nusselt number (heat transfer rate) and local Sherwood number (mass transfer rate) plotted in Figs. 1–9.

The physical appearance of temperature distribution $\theta(\eta)$ and $\varphi(\eta)$ is obtained respectively under the influence of various values of Prandtl number Pr as shown in Fig. 1. This result is obtained for the two different cases of PEST and PEHF respectively elaborated by $\theta(\eta)$ and $\varphi(\eta)$. It is determined that rising values of the Prandtl number Pr improves the temperature profiles for both cases of PEST and PEHF, although Pr is more effective in case of PEHF as compared to the PEST case. Figs. 2 and 3 are plotted to observe the characteristics of temperature distribution $\theta(\eta)$ under the influence of various values of N_t and Q respectively, whereas the rest of the parameters are chosen to be unvarying. The results have been obtained individually for both PEST and PEHF case represented by $\theta(\eta)$ and $\varphi(\eta)$ Both $\theta(\eta)$ and $\varphi(\eta)$ respectively rises with the scaling up of N_t as determined in Fig. 2. It is least for the value zero of N_t and rises extremely for the higher values of $N_t = 1.5$. The similar influence of the parameter Q is detected in Fig. 3, where both $\theta(\eta)$ and $\varphi(\eta)$ boosts with the magnifying values of Q.

The concentration profiles $h(\eta)$ for the different values of Le and Nb have been obtained respectively in Figs. 4 and 5. Both in case of PEST and PEHF, it appears that $h(\eta)$ boosts with the ever-increasing values of Le respectively reported in Fig. 4a and b. The reverse of this case is detected in Fig. 5a and b where $h(\eta)$ profile declines with the improvement of Nb. The graphical output of the flow velocity for the several values of the β have been plotted in Fig. 6. This result does not depend on the choice of PEST and PEHF case, because the momentum equation is not coupling with the heat and concentration equations. It has been found that $f'(\eta)$ declines with the escalating values of both β which confirms that the flow speed is minimum when the magnetic field is fixed at the right angle.

The friction drags C_f is obtained for the different values of K with respect to the increasing rate of mass suction graphically portrayed in Fig. 7. This figure clarifies that C_f controls with the strength of porosity parameter K. It is maximum when K is neglected ($K = 0$). At the same time, it continuously decreases with the strength of the suction and vice versa. The heat transfer rate Nu is checked for the different values of N_b against the continuous variation of suction as shown respectively in Fig. 8. It appears that Nu decreases with the increase of N_b. Moreover, it continuously increases with the increasing rate of suction, since it causes heat drain which consequently rises the rate of heat transfer. Thus, suction could be applied to manage the temperature of different processes. Fig. 9 addresses the characteristics of Sherwood number Sh for the different values of L_e which are plotted with the continuous variation of the suction. This figure certifies that Sh increases with the rising values of L_e. It also increases with the continuous increment of mass suction. In order to verify our numerical solutions with the solutions of Nadeem et al. [Aa], we have determined the numerical values of the skin friction coefficient which are comparatively presented in Table 1. These numerical values of C_f are obtained for the same parametric values of both studies which coveys these studies towards the same situation. In view of this table we can say that our results are in excellent agreement with the results of Nadeem et al. [39].

4. Conclusion

- For both PEST and PEHF case, the temperature rises with the scaling up of N_t, Pr and Q.
- Both in case of PEST and PEHF, $h(\eta)$ boosts with the increasing values of Le and declines with the improvement of Nb.
- The velocity $f'(\eta)$ declines with the escalating values of both β and K.
- The friction drags C_f controls with the strength of magnetic field and the higher values of K.
- The heat transfer rate Nu reduces with the rising values of N_b as well as it enhances with the rising values of N_t.
- The Sherwood number Sh enhances with the rising values of Pr and L_e.

Author agreement

This is stated that the contents of the article entitled "**Heat and mass transfer in MHD Williamson nanofluid flow over an exponentially porous stretching surface**" is neither accepted nor published in any journal. The author will be responsible for any problem about article publication or acceptance if found in any journal. If further assistance needed, let me know.

Declaration of competing interest

Author have no conflict of interest for this submission.

Acknowledgements

We would like to thank the reviewers for their valuable suggestions and comments.

References

[1] B.C. Sakiadis, Boundary layer behavior on continuous solid flat surfaces, American Institute of Chemical Engineers Journal 7 (1961) 26–28.
[2] F.K. Tsou, E.M. Sparrow, R.J. Goldstein, Flow and heat transfer in the boundary layer on a continuous moving surface, Int. J. Heat Mass Tran. 10 (1967) 219–235.
[3] L.E. Erickson, L.T. Fan, V.G. Fox, Heat and mass transfer in the laminar boundary layer flow of a moving flat surface with constant surface velocity and temperature focusing on the effects of suction/injection, Ind. Eng. Chem. Fundam. 5 (1966) 19–25.
[4] M.R. Khan, Numerical analysis of oblique stagnation point flow of nanofluid over a curved stretching/shrinking surface, Phys. Scripta 95 (10) (2020), 105704.
[5] X. Li, A.U. Khan, M.R. Khan, S. Nadeem, S.U. Khan, Oblique stagnation point flow of nanofluids over stretching/shrinking sheet with Cattaneo–Christov heat flux model: existence of dual solution, Symmetry 11 (9) (2019) 1070.
[6] M.R. Khan, M. Li, S. Mao, R. Ali, S. Khan, Comparative study on heat transfer and friction drag in the flow of various hybrid nanofluids effected by aligned magnetic field and nonlinear radiation, Sci. Rep. 11 (1) (2021) 1–14.
[7] M.R. Khan, K. Pan, A.U. Khan, N. Ullah, Comparative study on heat transfer in CNTs-water nanofluid over a curved surface, Int. Commun. Heat Mass Tran. 116 (2020), 104707.
[8] S. Nadeem, A.U. Khan, MHD oblique stagnation point flow of nanofluid over an oscillatory stretching/shrinking sheet: existence of dual solutions, Phys. Scripta 94 (7) (2019), 075204.
[9] D. Qaiser, Z. Zheng, M.R. Khan, Numerical assessment of mixed convection flow of Walters-B nanofluid over a stretching surface with Newtonian heating and mass transfer, Thermal Science and Engineering Progress 22 (2020), 100801.
[10] M.R. Khan, K. Pan, A.U. Khan, S. Nadeem, Dual solutions for mixed convection flow of SiO2− Al2O3/water hybrid nanofluid near the stagnation point over a curved surface, Phys. Stat. Mech. Appl. 547 (2020), 123959.
[11] M. Sheikhlesami, R. Ellahi, Three-dimensional mesoscopic simulation of magnetic field effect on natural convection of nanofluid, Int. J. Heat Mass Tran. 89 (2015) 799–808.
[12] R.U. Haq, Z.H. Khan, W.A. Khan, Thermophysical effects of carbon nanotubes on MHD ow over a stretching surface, Phys. E Low-dimens. Syst. Nanostruct. 63 (2014) 215–222.
[13] R. Mehmood, S. Nadeem, S. Massod, Effects of transverse magnetic field on a rotating micropolar fluid between parallel plates with heat transfer, J. Magn. Magn Mater. 40 (2016) 1006–1014.
[14] A. Borrelli, G. Giantesio, M.C. Patria, MHD oblique stagnation-point flow of a Newtonian fluid, Z. Angew. Math. Phys. 63 (2) (2012) 271–294.
[15] S. Nadeem, M.R. Khan, A.U. Khan, MHD stagnation point ow of viscous nanofluid over a curved surface, Phys. Scripta 94 (11) (2019), 115207.
[16] D. Pal, G. Mandal, Hydromagnetic convective–radiative boundary layer flow of nanofluids induced by a non-linear vertical stretching/shrinking sheet with viscous–Ohmic dissipation, Powder Technol. 279 (2015) 61–74.
[17] S.M. Mousavi, A.A.R. Darzi, O. ali Akbari, D. Toghraie, A. Marzban, Numerical study of bio magnetic fluid flow in a duct with a constriction affected by a magnetic field, J. Magn. Magn Mater. 473 (2019) 42–50.
[18] R. Sarlak, S. Yousefzadeh, O.A. Akbari, D. Toghraie, S. Sarlak, The investigation of simultaneous heat transfer of water/Al_2O_3 nanofluid in a close enclosure by applying homogeneous magnetic field, Int. J. Mech. Sci. 133 (2017) 674–688.
[19] S. Foroutan, A. Haghshenas, M. Hashemian, S.A. Eftekhari, D. Toghraie, Spatial buckling analysis of current-carrying nanowires in the presence of a longitudinal magnetic field accounting for both surface and nonlocal effects, Phys. E Low-dimens. Syst. Nanostruct. 97 (2018) 191–205.
[20] D. Toghraie, S.M. Alempour, M. Afrand, Experimental determination of viscosity of water-based magnetite nanofluid for application in heating and cooling systems, J. Magn. Magn Mater. 417 (2016) 243–248.
[21] P. Barnoon, D. Toghraie, F. Eslami, B. Mehmandoust, Entropy generation analysis of different nanofluid flows in the space between two concentric horizontal pipes in the presence of magnetic field: single-phase and two-phase approaches, Comput. Math. Appl. 77 (3) (2019) 662–692.
[22] C.W. Zhang, J.P. Ou, J.Q. Zhang, Parameter optimization and analysis of a vehicle suspension system controlled by magnetorheological fluid dampers, Struct. Contr. Health Monit. 13 (5) (2006) 885–896.
[23] X.Q. Wang, A.S. Mujumdar, Heat transfer characteristics of nanofluids: a review, Int. J. Therm. Sci. 46 (1) (2007) 1–19.

[24] S.U.S. Choi, Enhancing thermal conductivity of fluids with nanoparticles, ASME Fluids Eng. Div. 231 (1995) 99–105.
[25] J. Boungiorno, Convective transport in nanofluids, J. Heat Tran. 128 (2006) 240–250.
[26] A.V. Kuznetsov, D.A. Nield, Natural convective boundary-layer flow of a nanofluid past a vertical plate, Int. J. Therm. Sci. 49 (2) (2010) 243–247.
[27] D.A. Nield, A.V. Kuznetsov, The Cheng–Minkowycz problem for natural convective boundary-layer flow in a porous medium saturated by a nanofluid, Int. J. Heat Mass Tran. 52 (25–26) (2009) 5792–5795.
[28] S. Chen, M.K. Hassanzadeh-Aghdam, R. Ansari, An analytical model for elastic modulus calculation of *SiC* whisker-reinforced hybrid metal matrix nanocomposite containing n *SiC* nanoparticles, J. Alloys Compd. 767 (2018) 632–641.
[29] X. Zhu, F. Lin, Z. Zhang, X. Chen, H. Huang, D. Wang, Z. Wei, Enhancing performance of a *GaAs/AlGaAs/GaAs* nanowire photodetector based on the two-dimensional electron–hole tube structure, N*ano Lett.* 20 (4) (2020) 2654–2659.
[30] M. Wang, L. Yang, B. Hu, J. Liu, L. He, Q. Jia, Z. Zhang, Bimetallic *NiFe* oxide structures derived from hollow P*NiFe* Russian blue nano box for label-free electrochemical biosensing adenosine triphosphate, Biosens. Bioelectron. 113 (2018) 16–24.
[31] C.L. Shen, Q. Lou, J.H. Zang, K.K. Liu, S.N. Qu, L. Dong, C.X. Shan, Near-infrared chemiluminescent carbon nanodots and their application in reactive oxygen species bioimaging, Adv. Sci. 7 (8) (2020) 885–896, 1903525.
[32] M. Afrand, D. Toghraie, N. Sina, Experimental study on thermal conductivity of water based Fe_3O_4 nanofluid: development of a new correlation and modeled by artificial neural network, Int. Commun. Heat Mass Tran. 75 (2016) 262–269.
[33] A.J. Chamkha, C. Issa, K. Khanafer, Natural convection from an inclined plate embedded in a variable porosity porous medium due to solar radiation, Int. J. Therm. Sci. 41 (1) (2002) 73–81.
[34] N. Hadidi, R. Bennacer, Y. Ould-Amer, Two-dimensional thermosolutal natural convective heat and mass transfer in a bi-layered and inclined porous enclosure, Energy 93 (2015) 2582–2592.
[35] W.A. Khan, J.R. Culham, O.D. Makinde, Combined heat and mass transfer of third grade nanofluids over a convectively heated stretching permeable surface, Can. J. Chem. Eng. 93 (10) (2015) 1880–1888.
[36] N. Freidoonimehr, M.M. Rashidi, S. Mahmud, Unsteady MHD free convective flow past a permeable stretching vertical surface in a nano-fluid, Int. J. Therm. Sci. 87 (2015) 136–145.
[37] S.M. Razi, S.K. Soid, A.S. Abd Aziz, N. Adli, Z.M. Ali, Williamson nanofluid flow over a stretching sheet with varied wall thickness and slip effects, In J. Phys. Conf. 1366 (1) (2019), 012007.
[38] S. Nadeem, S.T. Hussain, Heat transfer analysis of Williamson fluid over exponentially stretching surface, Appl. Math. Mech. 35 (4) (2014) 489–502.
[39] S. Nadeem, S.T. Hussain, C. Lee, Flow of a Williamson fluid over a stretching sheet, Braz. J. Chem. Eng. 30 (3) (2013) 619–625.